ISPRS Journal of Photogrammetry and Remote Sensing 128 (2017) 170–181

Contents lists available at ScienceDirect

ISPRS Journal of Photogrammetry and Remote Sensing

journal homepage: www.elsevier.com/locate/isprsjprs

An operational method for the disaggregation of land surface temperature to estimate actual evapotranspiration in the arid region of Chile

L. Olivera-Guerra [a,b,*], C. Mattar [a], O. Merlin [b], C. Durán-Alarcón [a,c], A. Santamaría-Artigas [a,d], R. Fuster [e]

[a] Laboratory for Analysis of the Biosphere (LAB), University of Chile, Santiago, Chile
[b] Centre d'Etudes Spatiales de la Biosphère (CESBIO), Toulouse, France
[c] Institut des Géosciences de l'Environnement (IGE), CNRS, Université Grenoble Alpes, 38400 Saint-Martin-d'Hères, France
[d] Department of Geographical Sciences, University of Maryland, College Park, MD 20742, USA
[e] Dept. Environmental Sciences, School of Agronomic Sciences, University of Chile, Santiago, Chile

ARTICLE INFO

Article history:
Received 24 September 2016
Received in revised form 15 March 2017
Accepted 27 March 2017
Available online 7 April 2017

Keywords:
LST
Disaggregation
Evapotranspiration
Arid region
Landsat-8
MODIS

ABSTRACT

Monitoring evapotranspiration in arid and semi-arid environments plays a key role in water irrigation scheduling for water use efficiency. This work presents an operational method for evapotranspiration retrievals based on disaggregated Land Surface Temperature (*LST*). The retrieved *LST*s from Landsat-8 and MODIS data were merged in order to provide an 8-day composite *LST* product at 100 × 100 m resolution. The method was tested in the arid region of Copiapó, Chile using data from years 2013–2014 and validated using data from years 2015–2016. In-situ measurements from agrometeorological stations such as air temperature and potential evapotranspiration (*ET0*) estimated at the location were used in the ET estimation method. The disaggregation method was developed by taking into account (1) the spatial relationship between Landsat-8 and MODIS *LST*, (2) the spatial relationship between *LST* and the Normalized Difference Vegetation Index (*NDVI*) at high spatial resolution (Landsat-8), and (3) the temporal variations along the year of both relationships aforementioned. The comparison between disaggregated *LST* at 100 m resolution and in situ *LST* measurements presents a coefficient of determination (r^2), in average, equal to 0.70 and a RMSE equal to 3.6 K. The disaggregated *LST* was used in an operational model to estimate the actual evapotranspiration (*ETa*). The *ETa* shows good results in terms of seasonal variations and in comparison to the evapotranspiration estimated by using crop coefficients (*kc*). The comparison between remotely sensed and in situ *ETa* presents an overall r^2 close to 0.67 and a RMSE equal to 0.6 mm day^{-1} for both crops. These results are important for further improvements in water use sustainability in the Copiapó valley, which is currently affected by high water demand.

1. Introduction

Evapotranspiration (*ET*) is one of the most important parameters of the hydrological cycle affecting water availability on the Earth's surface. During the last decades, several works have been documented the critical importance of ET for agricultural irrigation scheduling (Porter et al., 2012; Senay et al., 2013), water resource availability (Oki and Kanae, 2006), hydrologic and meteorological forecasts (Findell et al., 2011) and climate change scenarios related to drought indexes (Gao et al., 2011). ET estimations are also crucial for management of water resource in areas of water scarcity since the actual rate of water use by vegetation can deviate significantly from potential ET rates (as regulated by atmospheric demand for water vapor) (Anderson et al., 2012). Thus, detailed spatial and temporal maps of ET provide power tools for decision makers and enable managers to more judiciously allocate available water for agricultural, urban, and environmental uses.

To estimate and quantify ET, it is necessary to account for diverse meteorological observations and land surface parameters such as the land surface temperature (LST). LST modulates the surface energy fluxes and it is key to estimating ET for monitoring crop water demand (Kalma et al., 2008; Li et al., 2009; Zhan

* Corresponding author at: Laboratory for Analysis of the Biosphere (LAB), University of Chile, Santiago, Chile.
E-mail address: olivera-guerrale@cesbio.cnes.fr (L. Olivera-Guerra).

http://dx.doi.org/10.1016/j.isprsjprs.2017.03.014
0924-2716/

et al., 2013; Cammalleri et al., 2014). In agricultural and heterogeneous natural systems, high variability of ET and LST can occur at scales of hundreds of meters or less. Thus, moderate-resolution satellite Thermal Infra Red (TIR) imagery is therefore required and essential to identify and fully understand water use and water availability at the field scale associated with specific crop types (Anderson et al., 2012; Senay et al., 2016).

The combination of *LST* and vegetation indexes at several time and spatial scales has been proven as a potential technique to disaggregate *LST* (DLST) to determine crop *ET*. Several *DLST* methods have been proposed in recent decades using various information sources available at low, medium or high spatial resolution, which are widely detailed in Zhan et al. (2013). Nevertheless, the Normalized Difference Vegetation Index (NDVI) based methods are still the most used operational approaches due to the availability of data at high spatio-temporal resolution. For instance, ALEXI, DisALEXI, DisTrad, TsHarp, among other algorithms (Kustas et al., 2003; Anderson et al., 2004; Agam et al., 2007; Bindhu et al., 2013; Cammalleri et al., 2014; Mukherjee et al., 2014).

Some variations of the NDVI based methods including phenology such as the robust disaggregation procedure proposed by Merlin et al. (2010, 2012) which account for the senescent vegetation fraction and soil moisture in addition to *NDVI*. These methods require additional parameters such as soil moisture, albedo, soil and vegetation temperatures, among others, which might be difficult to implement in an operational structure. There are other simple methods based on a subtraction approach that merge the spatial detail of higher-resolution imagery with the temporal change observed in coarser or moderate-resolution imagery (Hong et al., 2011; Kim and Hogue, 2012). The methods mentioned above can be applied to *ET* or soil moisture retrievals in order to estimate the surface energy balance (*SEB*) at better spatial resolutions, as well as to crop water management (Sobrino et al., 2012; Mattar et al., 2014). However, DLST method must be adapted over arid zones where high seasonal phenology in addition to thermal amplitude is evidenced in large areas.

Remote Sensing monitoring of semi-arid or arid regions target cultivated areas surrounded by barren conditions (e.g. deserts) which can impact on *DLST* and therefore in *ET* quantification. The proportion of bare soil observed in a given pixel during a year can affect the crop vegetated fraction increasing the *LST* and affecting *ET* and water requirements. Hence, *DLST* approaches concerning the spatial resolution over arid or semi-arid regions by using operational methods should be capable to monitor crop water consumption and usage accounting the seasonal variations. Despite the fact that there are some works on complex heterogeneous and semi-arid regions (Zhu et al., 2010; Weng et al., 2014), these methods are not simple in their application and present shortcomings in the operational mode such as the use of search windows to select similar pixels and to perform a sensitivity analysis before modeling (Weng et al., 2014).

In Chile, a persistent rainfall deficit has prevailed in the central zone since 2010 leading with a decline in water reservoirs generating a megadrought without precedents (Boisier et al., 2016). In the arid region of Chile, such as the Copiapó valley, the water resources availability has declined in addition to the water demand owing to agricultural and mining activities. The arid region of Copiapó is one of the most important agricultural areas of Chile and demands large amounts of water (4856 L/s equal to 59% of the total demand in the Copiapó; Bravo, 2013). Thus, it is of crucial importance that the water demand be determined and monitored and the water use efficiency be improved in this zone. Therefore, the main objective of this work is to present an operational *DLST* approach for estimating the actual evapotranspiration (*ETa*) over an arid or semi-arid region in Chile. This manuscript is structured as follows: Section 2 presents the study area and data. Section 3 describes the method proposed in this work. Section 4 presents the results and analysis and finally, Sections 5 and 6 provide the discussion and conclusions, respectively.

2. Study area and data sets

2.1. Study area

The study area belongs to the Copiapó Valley located in the arid region of Atacama, Chile. The whole valley has an area of about 18538 km^2 divided in longitudinal sectors from the Los Andes Highlands (sector 1) to the coast (sector 6) (Fig. 1). The study area has a surface of about 1670 km^2, and is located in the flat lands of sectors 5 and 6. It is an agricultural area mainly covered by olives, vineyards, pomegranates and natural vegetation (Fig. 1). The climate is semi-arid to arid with low mean annual precipitation (28 mm) and hot and dry summers (December, January and February), which coincide with the vineyard's growing season, and cold and dry winters (June, July and August). Despite the Copiapó Valley's proximity to the Atacama Desert, the zone located in sector 5 and 6 is highly covered with clouds for several days per year, which might affect the *ETa* measurements and the availability of optical remote sensing imagery. In terms of water resources, the Copiapó Valley is characterized by acute water scarcity mainly attributed to the low annual precipitation and the systematic stress put onto the aquifer by water consumers, mainly agriculture and mining (Oyarzún and Oyarzún, 2011; Valdés-Pineda et al., 2014; Suarez et al., 2014). This situation has brought about the Copiapó Valley's current critical situation, resulting from the extraction of water in recent decades, which has risen to rates greater than the natural replenishing of the aquifer (demand equal to 8222 L/s over a replenishing equal to 6347 L/s; Bravo, 2013), thus increasing the pressure for water resources and generating a new regional scenario for water use efficiency.

2.2. In situ data

In this work, in situ data derived from meteorological stations generated by the "Grupo de Estudios del Agua (GEA)" (www.agroclima.cl), in addition to LAB-network (here in-after LAB-net) (Mattar et al., 2016) data sets, were used. The GEA meteorological data sets were provided by 12 meteorological stations in the Copiapó Valley, four of which are located in the study area of this work. These stations were located in vineyards and olives orchards, and they provide basic meteorological parameters. The reference evapotranspiration (*ET0*) from ASCE standardized of a short crop and air temperature (*Ta*) between January 2013 and December 2014 were processed from the GEA network and used in this work.

In addition, in order to complement the GEA meteorological stations, data from two meteorological and radiative flux stations from LAB-net were also used. To this end, *ET0*, *Ta*, *infrared thermal, global and net radiation* (*Rg*, *Rn*) provided at olive orchards and vineyards crops were processed between July 2014 to December 2014, totaling 6 stations in the study area. These stations were used to generate the calibration and the partial evaluation of the *ETa* retrieval approach. On the other hand, LAB-net data from years of 2015 and 2016 was used to validate the *DLST* and *ETa*. The LAB-net station over olives orchards is located in a plot of land measuring about 17 hectares with a fraction vegetation cover of 25% distributed uniformly. Whereas the LAB-net station over vineyards is located in an area of 28 hectares with a homogeneous fraction vegetation cover.

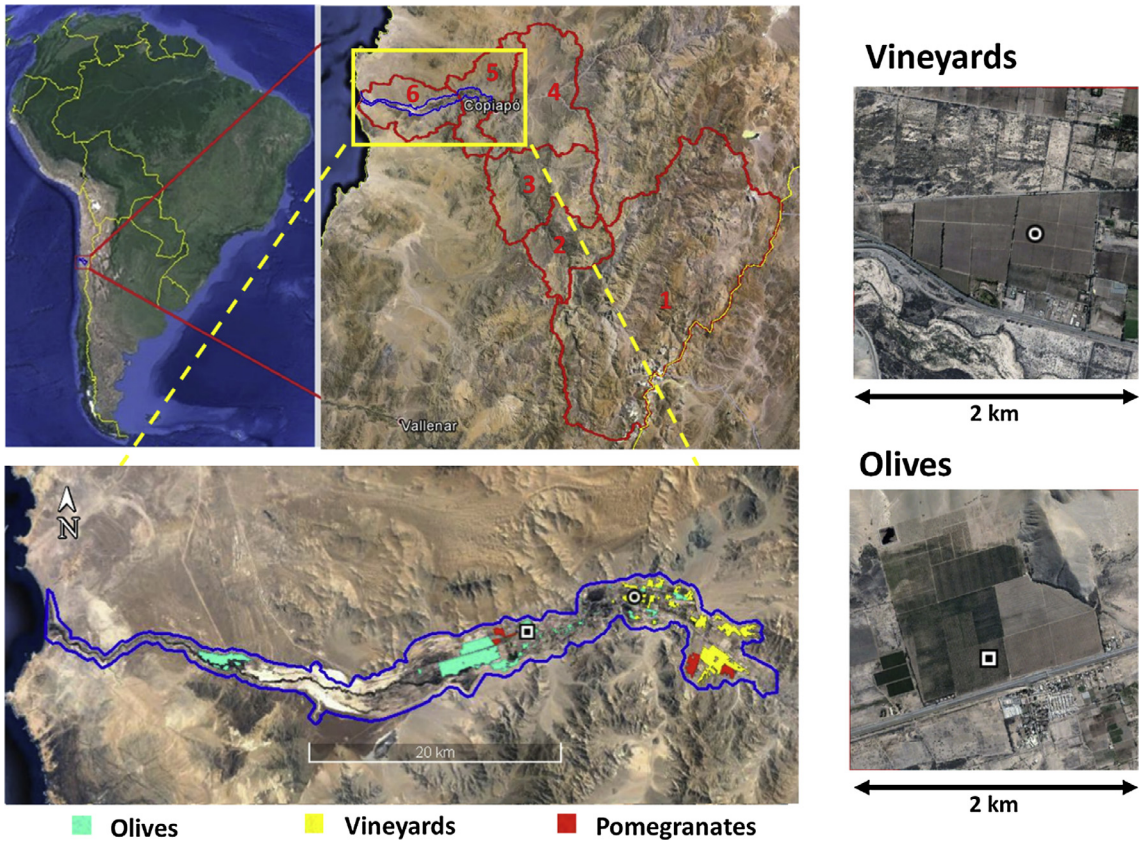

Fig. 1. Copiapó Valley divided in 6 sectors (red line) over which the study area (blue line) and the meteorological station over olive and vineyard crops (square and circle, respectively) are located in the sectors 5 and 6. In the figure the land cover of the main crops are shown: olives, vineyards and pomegranates. (For interpretation of the references to colour in this figure legend, the reader is referred to the web version of this article.)

2.3. Remote sensing data

To generate an operational approach, Landsat-8 and MODIS data products were used. In the case of Landsat-8, 25 clear sky images for Path 1 and Row 79 acquired for years 2013 (11 images) and 2014 (14 images) were used to develop and calibrate the proposed methodology. In addition, 21 clear sky images for years 2015 (9) and 2016 (12) for validation of Landsat-8 LST and for comparison of the DLST estimates. For the case of MODIS, water vapor content from the MOD05 and MOD07 product V5.0 was used in the estimation of the *LST* from Landsat-8. Moreover, the MODIS/Terra composite 8-day *LST* product (MOD11A2 V5.0) at 1 km spatial resolution and the MODIS/Terra composite 16-day normalized difference vegetation index *NDVI* (MOD13Q1 V5.0) at 250 m spatial resolution were also used in the *DLST* approach for the calibration (2013–2014) and validation (2015–2016) of *DLST* and *ETa* estimates.

3. Methodology

3.1. Disaggregation LST (DLST)

First of all, the *LST* from Landsat-8 was estimated by using the band 10 through the Single-channel (SC) algorithm described in Jiménez-Muñoz et al. (2014) and based on the work proposed by Sobrino et al. (1996) and is represented as follows:

$$LST = \gamma\left[\frac{1}{\varepsilon}(\varphi_1 \cdot L_{sen} + \varphi_2) + \varphi_3\right] + \delta \quad (1)$$

where ε is the surface emissivity, (φ, δ) are two parameters which depend of the at-sensor brightness temperature and the thermal band, and φ_1, φ_2 and φ_3 are approximation of the atmospheric functions versus the atmospheric water vapor content W from a second-order polynomial fit, whose coefficients are obtained from radiative transfer simulation using the GAPRI database (Mattar et al., 2015) and the W was derived from the daily MOD05 product. The emissivity ε was estimated according to the simplified *NDVI* thresholds method proposed by Sobrino et al. (2008), which requires *NDVI* and knowledge of the soil-emissivity spectrum corresponding to the soils of the study area. The soil emissivity was calculated by using the soil types from the ASTER spectral library (Baldridge et al., 2009), which belong to aridisol and entisol and were convoluted by using the relative spectral response for the Landsat-8 thermal band 10 using the RSR calculator (Durán-Alarcón et al., 2014). Finally, the *NDVI* threshold was 0.15 and 0.80 for the minimum and maximum, respectively. Both MODIS and Landsat-8 *LST* data were filtered by cloud mask using the Quality Control (QC) of both MODIS and Landsat-8. Both Landsat-8 and MODIS were spatially matched in order to extract the study area from both images and for the study period between 2013 and 2014.

The disaggregation method was developed by taking into account (1) the spatial relationship between *LST* and the Normalized Difference Vegetation Index (*NDVI*) at high spatial resolution (Landsat-8), (2) the spatial relationship between Landsat-8 and MODIS *LST*, and (3) the temporal variations along the year of both relationships aforementioned. The following sections describe these relationships and the methodology to merge them to obtain

the disaggregation LST product at Landsat spatial resolution and at higher temporal frequency of MODIS.

3.2. Relationship between LST and NDVI

The temporal variability of LST shows a strong seasonality (Weng et al., 2008) which its seasonal change can be modeled using the annual temperature cycle approximated by a sinusoidal function (Bechtel, 2012). In a similar way, the vegetation indices as NDVI present a strong seasonality which have been widely used to describe the phenological cycles of different ecosystems at different spatial resolution (Cheema and Bastiaanssen, 2010; Duchemin et al., 1999; Li et al., 2010; Liu et al., 2017). The annual variability of both NDVI and LST can be evidenced at both field and watershed scale and can be monitored at the high spatial resolution of Landsat. Based on the strong seasonality of LST and NDVI, the variability of the relationship between *LST* and *NDVI* throughout the year was considered by using the seasonal behavior of the linear regression parameters derived from Landsat 8 imagery. The intercept and the slope of the *LST–NDVI* relationship are controlled by a wide range of factors, such as the fractional vegetation cover, surface soil moisture variability and meteorological factors (Nemani et al., 1993). The regression parameters could be fitted to a sinusoidal function due mainly to the annual temperature cycle and the seasonal changes of differences of temperature between soil and vegetation. The cloud-free images available to two years (2013–2014) were used in order to provide information of a complete annual cycle and taking into account the low temporal frequency of sensors as Landsat-8. The Landsat-8 *NDVI* was resampled to the same spatial resolution of Landast-8 *LST*.

Because an ordinary least square regression algorithm lacks robustness and is sensitive to outliers (Rousseeuw, 1984), some authors have proposed overcoming this problem by using subpixel variability based sampling (co-efficient of variation <25%) (Agam et al., 2007; Kustas et al., 2003) or using least median square (LMS) regression and Projection Adjustment by Contribution Estimation (PACE) regression for more heterogeneous landscapes because these methods are less sensitive to outliers (Mukherjee et al., 2014). In this work, we propose a new method to describe the linear regression between LST and NDVI. This was carried out using the mean LST values derived from NDVI classes separated by 0.01 step forward. This technique was used to overcome the sensitive to extreme value or outliers in a robust and efficient way and in order to obtain a seasonal behavior of regression parameter, which would be not possible observe by using all the scatter data in the feature space plot. The latter is due to the influence of different factors (mentioned above) that often results in a wide range of LST for a given value of NDVI, thus leading to an imprecise quantification of the slope of the NDVI–LST relationship (Bindhu et al., 2013).

The intercept and the slope (*a, b* respectively) obtained for the calibration period (2013–2014) were adjusted by using a sinusoidal function to estimate *a* and *b* every 8 days (a_{8day} and b_{8day}, respectively) throughout the year. An invariant spatial scale between 100 m and 250 m was assumed for modeling the linear coefficients in order to obtain a disaggregated *LST* every 8 days at 250 m from the composite 16-day MODIS *NDVI* product, accounting for the seasonal vegetation behavior described as follows:

$$LST_{250m\_8day} = a_{8day} + b_{8day} \cdot NDVI_{MOD_{250m\_16day}} + error_{100m\_8day} \quad (2)$$

where the subscripts 250 m and 8 day denotes the spatial and temporal resolution, respectively; a_{8day} and b_{8day} are the coefficients of the linear regression interpolated each 8 days for the whole image. *NDVI* 16-day composite was used for two corresponding 8-day period. To estimate LST using the LST – NDVI relationship the error pixel-by-pixel between the LST observed by Landsat 8 and the LST modeled were linear fitted. This error was obtained for each Landsat 8 image and then a second order polynomial fit was applied on a pixel-by-pixel basis to estimate an error each 8 days ($error_{100m\_8day}$).

3.3. Relationship between MODIS and Landsat-8 LST

On the other hand, the MODIS *LST* was resampled from 1 km to 100 m resolution by using nearest neighbors in order to estimate a seasonal factor which considers the relationship pixel by pixel between MODIS resampled image and Landsat-8 (4). This factor has a seasonal pattern and can be used as a partial disaggregation between Landsat-8 and MODIS following the size of the most representative crops in the study area.

$$\omega_{8day\_100m}(x,y,t) = \frac{LST_{L8\_100m}(x,y,t)}{LST_{MOD\_8day\_1km}(x,y,t)} \quad (3)$$

The seasonal factor $\omega_{8day\_100m}(x,y,t)$ varies according to differences of annual temperature cycle at coarse and fine scale, which is modulated by the specific LST temporal profiles at both scales. These differences can be mainly due to the different land cover at Landsat spatial-resolution (~100 m) and a coarser spatial-resolution (~1 km). For instance, homogeneous land covers, such as bare soil, will show low temporal differences at MODIS or Landsat-8 spatial resolution since the land cover is the same during the whole year, and the seasonal pattern will show a slow temporal variation. However, for heterogeneous land cover such as crops, several phenology stages will be evidenced and therefore, a high impact on the proportion of vegetation cover can be observed in MODIS or Landsat-8 pixel. In this case, $\omega_{8day\_100m}(x,y,t)$ demonstrates a crop seasonal behavior which modulates the *LST* between Landsat-8 and MODIS. The $\omega_{8day\_100m}(x,y,t)$ was calculated assuming a constant proportion of the land cover types contained in a given pixel. Once the factor $\omega_{8day\_100m}(x,y,t)$ was estimated for the whole calibration period, it was interpolated every 8 days for the whole year in order to process the *LST* from MODIS at 1 km resolution to Landsat-8 for 8 days (4).

$$LST_{8day\_100m} = \omega_{8day\_100m} \cdot LST_{MOD\_8day\_1km} \quad (4)$$

Once the relationship between LST – NDVI and Landsat-8 – MODIS was determined to estimate a product of *LST* at 250 m and 100 m each 8 days (LST_{8day_100m} and LST_{8day_250m} respectively), a combination of them were applied to generate a final and robust disaggregated *LST* at 100 m and 8 days ($DLST_{8day\_100m}$) as follow:

$$DLST_{8day\_100m} = LST_{8day\_100m} + \langle LST_{250m\_8day} - \langle LST_{8day\_100m} \rangle_{250m} \rangle_{100m} \quad (5)$$

with $\langle LST_{8day\_100m} \rangle_{250m}$ being the average of LST_{8day_100m} within each 250 m pixel resolution and $\langle\ \rangle_{100m}$ being the resampling from 250 m to 100 m resolution by using nearest neighbors in order to correct the product LST_{8day_100m} by the difference between LST_{8day_250m} and $\langle LST_{8day\_100m} \rangle_{250m}$. The final $DLST_{8day\_100m}$ retrieval can be performed operationally that can be very useful as application to surface energy budget. In this work, the $DLST_{8day\_100m}$ was used in an operational surface energy balance method to estimate the *ETa*, which is described below.

3.4. Estimation of actual evapotranspiration

The *ETa* was estimated by using the *Operational Simplified Surface Energy Balance* (*SSEBop*) developed by Senay et al. (2013) and evaluated in this study area by Olivera-Guerra et al. (2014). The *SSEBop* approach estimates the pixel-by-pixel evaporative fraction (*EF*) by using "hot/dry" and "cold/wet" reference values. To

estimate *ETa* routinely, the only data needed for this method are *LST*, daily maximum air temperature (*Ta*), and *ET0*.

This model relies on the simplification of the surface energy balance process which is mainly driven by the available net radiation (*Rn*). Since thermal remote sensing is conducted under clear-sky conditions, the *SSEBop* method assumes a location- and date-specific constant temperature difference (*dT*) between the hot/dry and cold/wet boundary reference points. *ETa* can be estimated using Eq. (6) as a fraction of the *ET0* as follows:

$$ET_a = EF \cdot k \cdot ET0 \tag{6}$$

where *ET0* is the green grass reference for the location; *k* is a coefficient that scales the *ET0* into the level of a maximum *ET* experienced by an aerodynamically rougher crop and *EF* is the evaporative fraction. Although a value of *k* between 1.0 – 1.25 is recommended (Allen et al., 2011; Senay et al., 2013; Senay et al., 2016), a value equal to 0.65 was used in this study, which was determined by Olivera-Guerra et al. (2014) to this domain area. This value is due to cover type mainly corresponding to vineyards and olive orchards, which often have a low fractional cover vegetation and whose maximum values of crop coefficient (*kc*) are equal to 0.70 and 0.65, respectively (Allen et al., 1998). The *EF* was estimated pixel-by-pixel according to the following equation:

$$EF = \frac{T_H - T_s}{T_H - T_C} = \frac{T_H - T_s}{dT} \tag{7}$$

where *Ts* is the *LST* downscaled at 100 m spatial resolution every 8 days. T_H is the estimated *Ts* at the idealized reference hot/dry condition of the pixel for the same time period, *Tc* is the estimated *Ts* at the idealized cold/wet reference point and the *dT* is the difference between *Th* and *Tc*. The cold boundary condition is derived as a correction of the *Ta*, whose correction coefficient was determined as a seasonal average between *Ts* and *Ta* on all pixels where *NDVI* is greater or equal to 0.75. A correction factor of 0.993 was established by using all Landsat imagery.

The predefined *dT* is solved from the *Rn* equation for a bare, dry soil where *ETa* is assumed 0 and sensible heat is assumed maximum (Bastiaanssen et al., 1998). It is calculated by using Eq. (8) and the assumptions of Senay et al., (2013).

$$dT = \frac{R_n r_{ah}}{\rho_a C_p} \tag{8}$$

where *Rn* is clear-sky net radiation (W m^{-2}); r_{ah} is the aerodynamic resistance to heat from a hypothetical bare and dry surface (sm^{-1}); ρ_a is the density of air (kg m^{-3}), estimated as a function of air pressure and temperature (Allen et al., 1998); *Cp* is the specific heat of air at constant pressure (1.013 kJ kg^{-1}K^{-1}). The r_{ah} was theoretically estimated through an iterative computation by implementing an energy budget for bare soil for the whole year according to Bastiaanssen (1995). According to this procedure, the average r_{ah} was equal to 113 sm^{-1}, which is very close to the value of 110 sm^{-1} determined by Senay et al. (2013).

3.5. Validation of LST and ETa

The validation of remotely sensed *LST* was carried out by comparing the *DLST* every 8 days and the *LST* measured in situ at LABnet stations. In order to compare the in-situ and the DLST at the 100 m scale, the thermal infrared sensor (Apogee SI-111®) was located at a height of 5 m and inclined to measure an area with the same fraction vegetation cover as the plot of land where the station is localized. To estimate the in situ *LST*, the radiometric temperature measured, by a step of 5 min, was converted to *LST* by using the following equation:

$$B(LST) = \frac{Lrad - (1-\varepsilon)Ldown}{\varepsilon} \tag{9}$$

where *Lrad* is the land leaving radiance (W m^{-2}) measured by a thermal radiometer, ε is the land surface emissivity, *Ldown* is the long-wave downwelling irradiance (W m^{-2}) and *B(LST)* is Planck's law for the *LST* (W m^{-2}sr^{-1}μm^{-1}). The *Ldown* was estimated using the methodology proposed by Jiménez-Muñoz et al. (2010), by processing a MOD07 profile into MODTRAN radiative transfer code and convoluting the downwelling irradiance spectra by using the Apogee SI-111® relative spectral response. The surface emissivity was acquired from the ASTER Global Emissivity Data Base (Hulley and Hook 2013) and the emissivity was converted from narrow band to a broad band by using the method proposed by Ogawa et al. (2003). Finally, the *LST* (K) was estimated by inverting Planck's law.

For the validation of *ETa*, the in situ *ET0* measured at the station located over the olive orchard and vineyard by a step of one hour were used. These *ET0* values were estimated at daily level and weighted by the *kc* estimated by the Direccion General de Aguas (2007) and Martínez and Tapia (2002) based on the FAO crop coefficient. The values of *kc* were estimated for the arid region of Atacama, changing during the seasons of the year. The mean *kc* values are presented in Table 1 for olives and vineyards and are crop site dependent which cannot be directly assimilated for the same crops in other regions of Chile. Finally, for the case of olives, the *kc* was weighted for fraction vegetation cover, which is equivalent to 25% during the whole year and the *kc* values were estimated to a vegetation cover equal to 50%.

To estimate the accuracy of the proposed *DLST* method and its application to *ETa* retrieval, the bias, standard deviation, RMSE and determination coefficient (r^2) were calculated for each station (olive and vineyards) between January 2015 and December 2016. This period was defined following the overflooding that occurred on 27th March 2015, which caused some damage to the irrigation system of the vineyards, as can be consequently seen in the crop growth after September 2015.

4. Results

4.1. Statistical relationship for LST – NDVI and Landsat-8 – MODIS

The *NDVI* and *LST* relationship was estimated to the 24 scenes available to the calibration period between 2013 and 2014. Fig. 2 represents the variability of scatterplot during a Landsat scene during winter and summer of 2013. In terms of seasonal variation, during winter the amplitude of *LST* is between 285 and 305 K, whereas in summer it varies between 290 K and 330 K. Meanwhile, the *NDVI* values mainly fall between 0.1–0.6 and 0.1–0.8 during winter and summer respectively. In summer, steeper slopes can be observed due to the greater temperature differences between soil and vegetation surface, as it is showed in Figs. 3 and 4.

The slope and intercept parameters were statistically adjusted for a sinusoidal shape (r^2 equal to 0.904 and 0.931, RMSE equal to 1.39 K and 2.63 K for slope and intercept, respectively). The estimated linear regression by the observed Landsat 8 and the simulated regression by the sinusoidal fit of slope and intercept match in terms of each statistical coefficient for each scene. This sinusoidal shape can be interpolated in order to obtain the parameters regression for the sinusoidal function to represent the whole year of *NDVI* and *LST* relationship for a Landsat scene. Indeed, Fig. 3 shows the scatter plots for the linear correlation between *NDVI* and *LST*.

In terms of the Landsat-8 and MODIS LST relationship, the fraction ω between both sensors can be fitted by a sinusoidal equation (Fig. 2), thus this parameter can be modeled for each day of the

Table 1
Vineyards and olives *kc* values.

	Jan	Feb	Mar	Apr	May	Jun	Jul	Aug	Sep	Oct	Nov	Dec
Vineyards	0.70	0.65	0.60	0.50	0.40	0.40	0.40	0.40	0.40	0.60	0.65	0.70
Olives	0.65	0.65	0.65	0.65	0.6	0.5	0.5	0.5	0.6	0.6	0.65	0.65

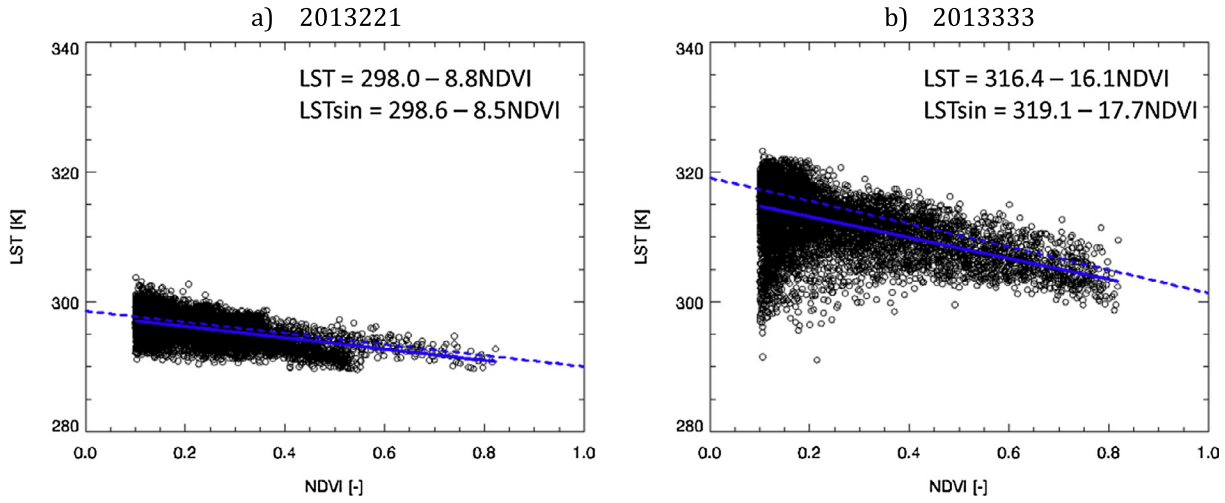

Fig. 2. Linear relationship between *LST* and *NDVI* by Landsat-8 image acquisition to winter (a) and summer (b). The equations are included for the linear regression from the observed Landsat-8 data (LST: solid line) and for the linear regression from the slope and intercept fitted to a sinusoidal function (LSTsin: dashed line).

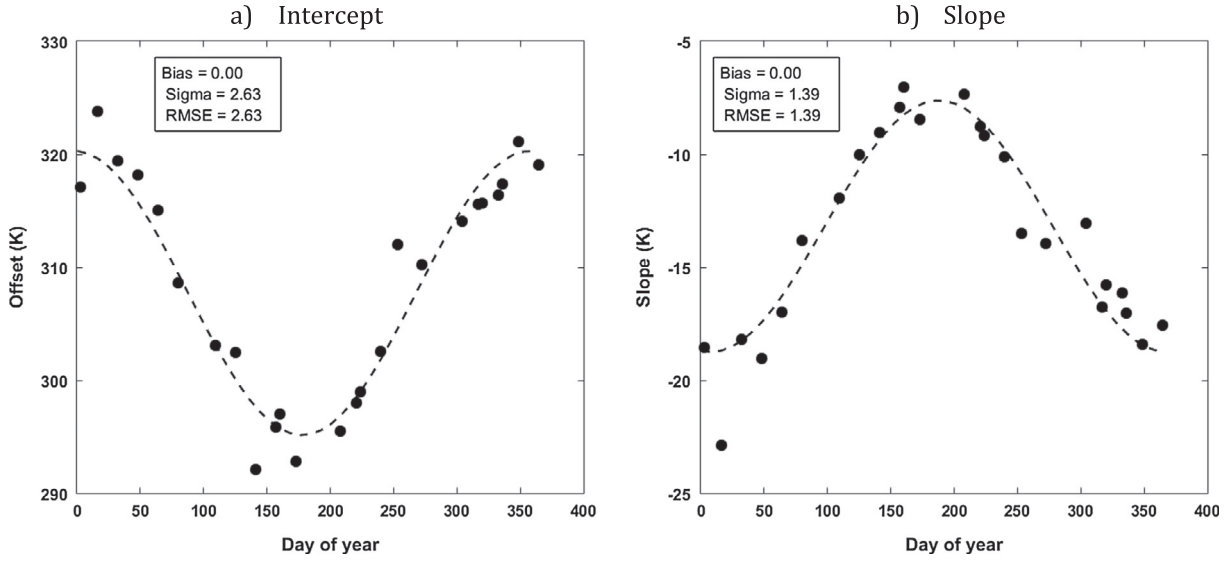

Fig. 3. Slope and intercept of the linear relationship between *LST* and *NDVI* from all Landsat image acquisition dates between 2013 and 2014 and its sinusoidal functions according to the day of year (dashed line).

year and the ω values for any obtained *DLST*. The ω can be obtained for each pixel according to the land cover type and the fraction of vegetation cover given in the Landsat-8 pixel at 100 m and in MODIS at 1 km spatial resolution. The difference of the fraction of vegetation cover between Landsat-8 and MODIS affects the annual amplitude of the ω, generating low amplitude for similar vegetation cover and high amplitude for a high difference of the vegetation cover between both Landsat-8 and MODIS pixels as presented in the case of olives and vineyards, respectively. This annual effect on ω can be also related to the land cover types variability within a MODIS pixel and its different phenological stages since the relationship between a fine and coarse resolution was revealed in terms of *LST* through the factor ω. The ω values can be closer to 1 in the case of olives and lower than 1 for vineyards because of during summer, during the maximum crop growth rate, the vegetation cover presents the highest values at Landsat-8 spatial resolution.

4.2. Disaggregation of LST (DLST)

Fig. 5 shows the disaggregated *LST* retrievals for a day on January (summer) and July (winter) used to obtain the *ETa* by using

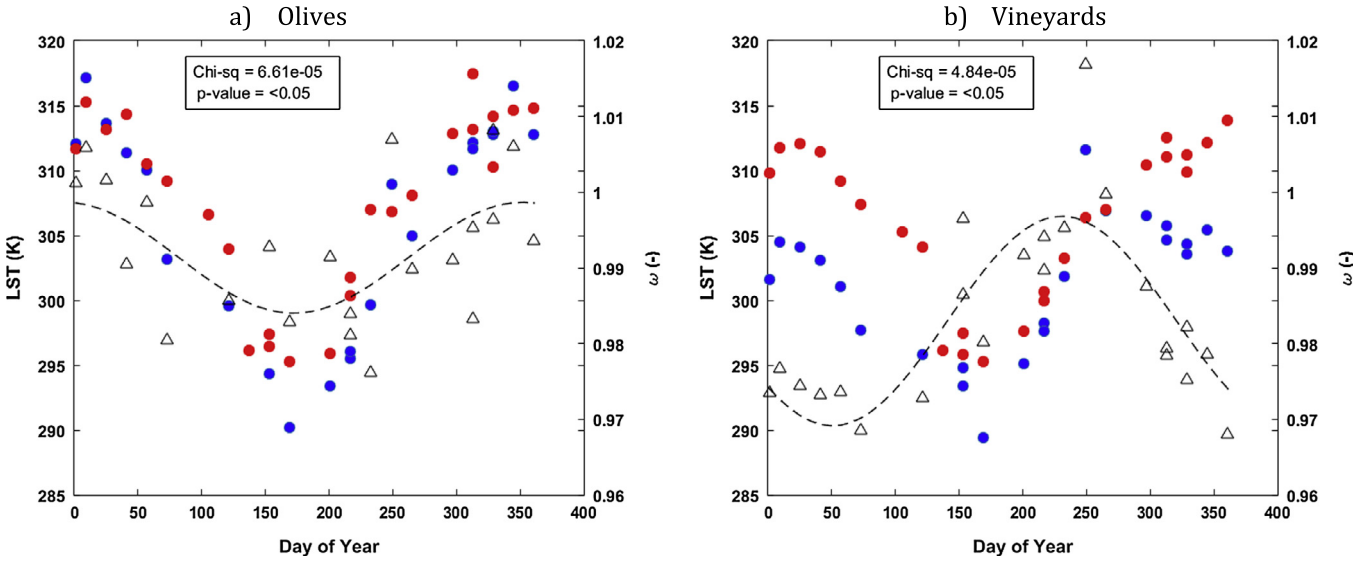

Fig. 4. *LST* from Landsat-8 overpass (blue circle), 8-day composite MODIS LST (red circle) and the ratio between Landsat-8 and *MODIS LST* (ω: triangle) for all Landsat image dates between 2013 and 2014. The sinusoidal functions of the ratio according to the day of the year (ω_{8day_100m}: dashed line). The graphs are shown for the pixel corresponding to the station located in olives (a) and vineyards (b). (For interpretation of the references to colour in this figure legend, the reader is referred to the web version of this article.)

MODIS and Landsat-8. The coarse (1 km) resolution MODIS *LST* can be used for a general characterization of the study area, where the most common feature is the bare soil surrounding the naturally vegetated and agricultural areas. For the case of *LST* retrieved at 250 m, the main vegetation orchards such as olives and vineyards can be distinguished in terms of low magnitudes of *LST*. Additionally, for January, the *LST* highlights the impact of the bare soil located on the boundary of the study area. However, when using the direct 1 km resolution *DLST* based on both MODIS and Landsat-8, the border reveals a high *LST* difference in comparison to the crops and orchards (±20 K and ±10 K for summer and winter, respectively). This can be also noticed for winter, where the vegetation of olive orchards located in the middle of the study area showed a *LST* noticeably lower than on the boundary. The use of both disaggregated *LST* from *NDVI* and by using the ω factor, resulted in a good characterization of olives orchards, vineyards and crops as they can be distinguished as the lower values. It is important to note that the riverbed of the Copiapó River can be also distinguished during winter since it gives the lowest *LST* values. Furthermore, the boundary's maximum *LST* values shown in the *NDVI–LST* relationship or by using the ω factor are smoothed in terms of the combination of both methodologies marking out the crop areas along the study area.

4.3. Evapotranspiration retrievals

The *ETa* estimated at 1 km and 100 m resolution for January and July is presented in Fig. 6. Over vineyards, a difference of about 10 mm 8 day^{-1} between the coarse and the fine pixel can be obtained during summer when using the *DLST* proposed method in comparison to MODIS. Other differences, though somewhat lower, are also obtained for Olives (±5 mm 8 day^{-1}) that are located in the central and western part of the study area. On the other hand, during July, the minimum threshold of *ETa* is evidenced over the riverbed, representing the lowest values of *ETa* in the whole study area (i.e. <2 mm 8 day^{-1}). The maximum values of *ETa* correspond to the vegetation orchards with partial vegetation cover such as olives or pomegranates. Vineyards did not show the maximum *ETa,* which seems to be consistent with the phenological stage of this crop. The *ETa* retrieved by MODIS is partially homogeneous during summer and winter, although the *ETa* retrieved by the *DLST* targeted the maximum values in summer and the minimum in winter, generating a heterogeneous *ETa* map which can be used to characterize the areas which need to be irrigated and useful for water requirements. However, for vineyards, there are significant differences when comparing seasonal periods such as summer and winter. For instance, during summer, a big difference in *ETa* can be seen by the influences of spatial resolution. These differences are close to 10 mm 8 day^{-1} when using MODIS or *ETa* from the *DLST* algorithm, although these differences are non-significative during winter.

As a partial evaluation with in situ measurements, Fig. 7 shows the times series for the *ETa* derived from *DLST* and 8-day composite MODIS LST over vineyards and olive orchards pixel at 100 m and 1 km resolution, respectively, and the *ET0* obtained from in situ measurements in the whole study area. It is important to note that maximum values are explained by the *ET0*, which seems to be lower when applying a *kc* in order to obtain *ETa*. For Olives, the vegetation cover fraction in addition to the proportions of land cover type at both 100 m pixel of DLST and 1 km pixel of MODIS are very close, thus the bare soil proportion is constant during all years and the vegetation fraction in both 100 m and 1 km pixel are very close. So, in the case of olives, when comparing the 1 km or 100 m resolution *ETa* with in situ measurements, there is no statistically significant differences ($p < 0.05$). The *ETa* from DLST and Landsat-8 overpass were compared show a good agreement in both olives and vineyards (r^2 equal to 0.67 in average for both crops), where the DLST is slightly underestimated in relation to Landsat-8 (bias equal to −0.05 mm day^{-1} and RMSE of 0.3 mm day^{-1} in average for both crops). It is important to note that *ETa* from DLST represent the average over 8 days whereas *ETa* from Landsat-8 overpass represent a clear-sky day, at least at the Landsat overpass. Therefore, this underestimation can be expected due to *ETa* from DLST can be represent the average over cloudy and clear-sky days.

4.4. Evaluation of LST and ETa

LST and *ETa* at 100 m and 8-days spatio-temporal resolution were simulated to the time series of 2015 and 2016 from the

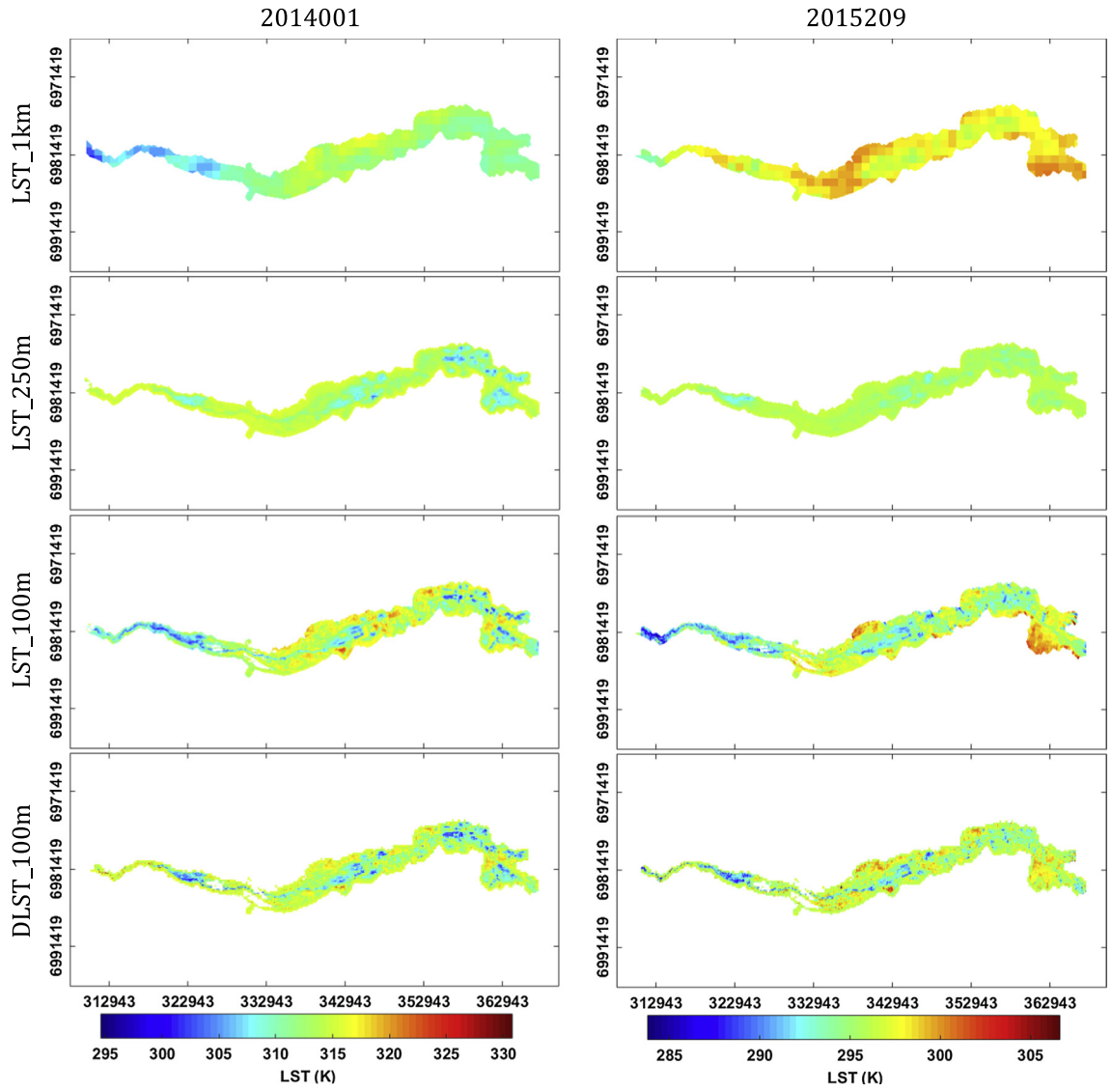

Fig. 5. Comparison between the composite 8-day MODIS *LST* (*LST* _1 km), the first product of disaggregated *LST* at 250 m from MODIS NDVI (*LST_250* m), the second product of *LST* at 100 m from MODIS *LST* (*LST_100* m) and the final disaggregated *LST* at 100 m (*DLST_100* m).

Eqs. (2), (3) and (5) by using the NDVI and LST MODIS composited product at 250 m and 1 km resolution, respectively. Note that Landsat imagery were used in the calibration period (2013–2014) and the evaluation period for 2015–2016. The time series of *LST* and *ETa* simulated from the operational approach and the in situ retrievals are presented in Fig. 8. The RMSE for *ETa* was estimated in 0.5 and 0.7 mm day^{-1} for olives and vineyards, respectively (Table 2). Meanwhile, the RMSE for *LST* was estimated lower than 3.6 K for both vineyards and olives. The *LST* during summer is overestimated closed to 4 and 6 K in olives and vineyards, respectively. The overestimation of LST could be attributed to the fraction vegetation cover which could generate rapidly changes in space as well as in time (Prata et al., 1995; Vauclin et al., 1982). This effect is related to the high complexity of surface temperature over the study area where more dense measurements are required with detailed spatial sampling (Li et al., 2013). On the other hand, high differences in *LST* over vineyards were observed during the summer 2015–2016 (December and January) corresponding to the maximum plant development to the vineyards. This was mainly attributed to the impact of irrigation on the crop since the drip system was damaged by the floods and it decreased the amount of water for the same period in the last years (2013 and 2014), which also explains the significant increase of LST in the plant development stage (September–November). The effect of the change in the irrigation can be evidenced by observing the NDVI that reached a value of 0.5 in summer 2015–2016 meanwhile the last years it was greater 0.7 for the same period. The differences in temperature retrieved during the summer season over vineyards might be attributed to misleading in surface emissivity values that can provoke errors of up to 4 K over arid and sparsely vegetated areas as described in Guillevic et al. (2014). Over olive orchards the fraction of vegetation cover is almost the same during the whole year, impacting on the amplitude of the *LST* between summer and winter and also in the comparison between in situ and *DLST*. Meanwhile in summer LST is overestimated, in winter is underestimated.

In spite of the differences observed between DLST and ground-based LST, a consistent agreement with Landsat-8 LST is observed, being also overestimated in summer season. Moreover, the statistics errors from DLST and Landsat-8 are very close for both olives and vineyards.

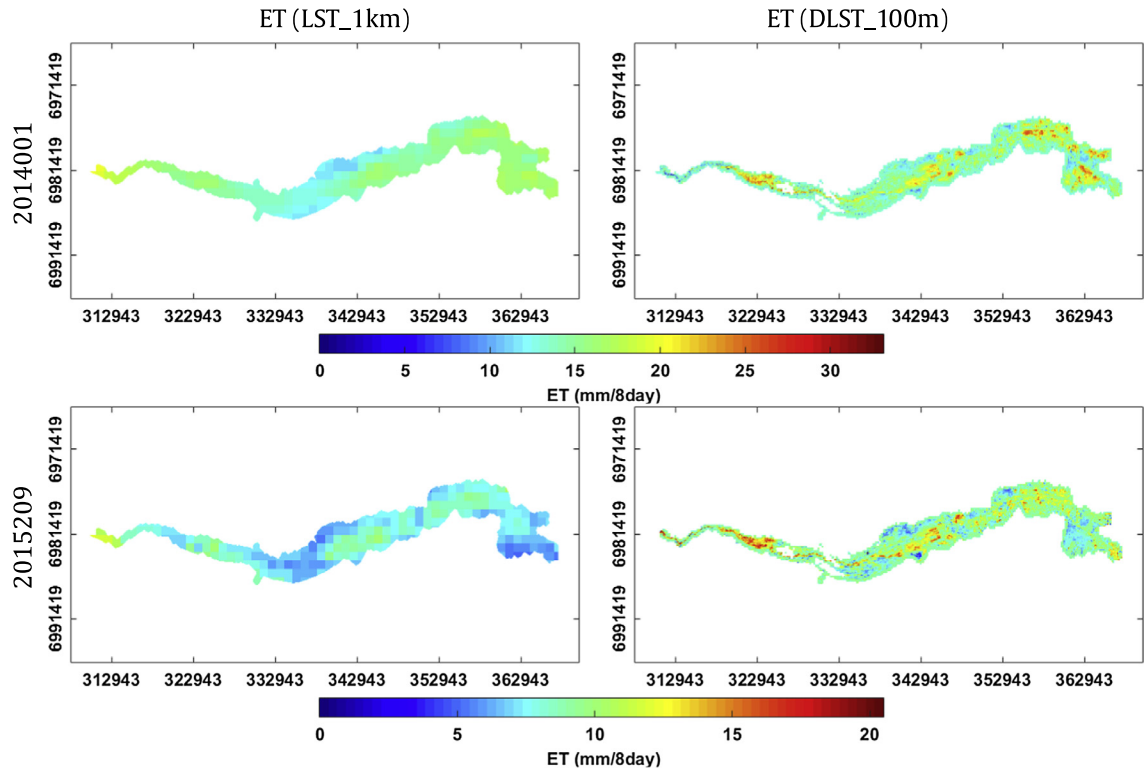

Fig. 6. Comparison between the composite 8-day *ETa* at 1 km and the disaggregated product at 100 m from MODIS *LST* at 1 km and the disaggregated *LST* product at 100 m, respectively.

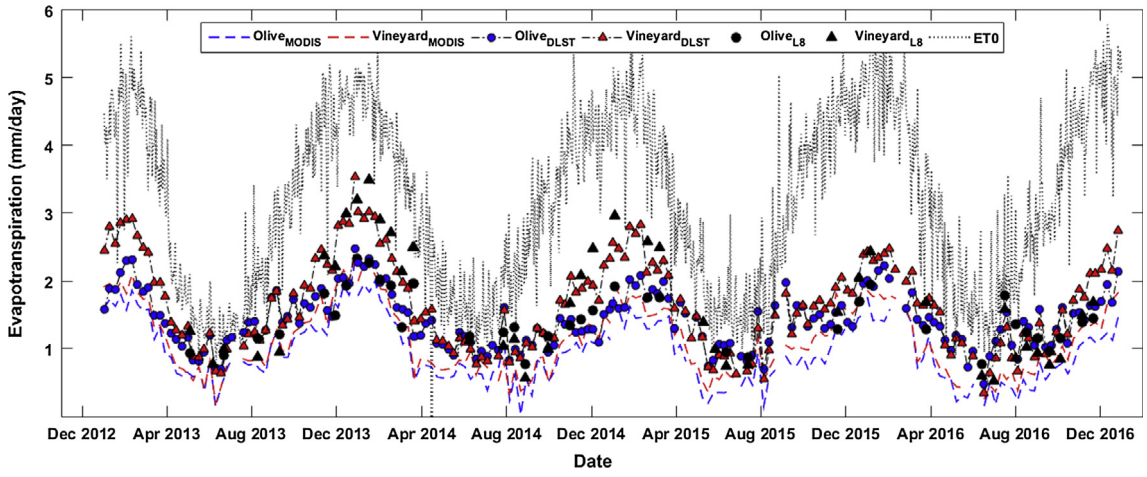

Fig. 7. *ETa* estimated over olive and vineyard station from different LST products. Subscript *MODIS* is for *ETa* from 8-day composite MODIS LST at 1 km, subscript *DLST* is for *ETa* from DLST proposed at 8-day and 100 m and *L8* is for *ETa* from Landsat-8 LST overpass at 100 m. *ETa* from DLST and MODIS are represented as the daily average over 8 days.

In terms of *ETa*, an important overestimation is evidenced during summer for vineyards showing the highest differences of the validation period reaching up to 1.4 mm day^{-1}. This difference could be attributed to the use of a *kc* for in situ *ETa* estimates under crop optimal conditions instead of the current crop which show some problems of water management (system irrigation) impacting the growing season and therefore lower NDVI values than the previous years. Therefore, it is possible that the *kc*-based *ETa* can be overestimated in vineyards for the summer periods after 2015. Another important result is the comparison between *ET0* and *ETa*, there is a high difference when comparing to *ET* in the arid zone, which shows an average difference greater than 1 mm day^{-1} during summer season accumulating 10 mm after 8 days. This is a key factor because in the study area, water irrigation scheduling programs are based on the *ET0*, which might overestimate the amount of water and therefore cause inefficiency in water usage.

5. Discussion

The sinusoidal annual relationship for *DLST* presented in this work performs well in terms of operational modes and applications

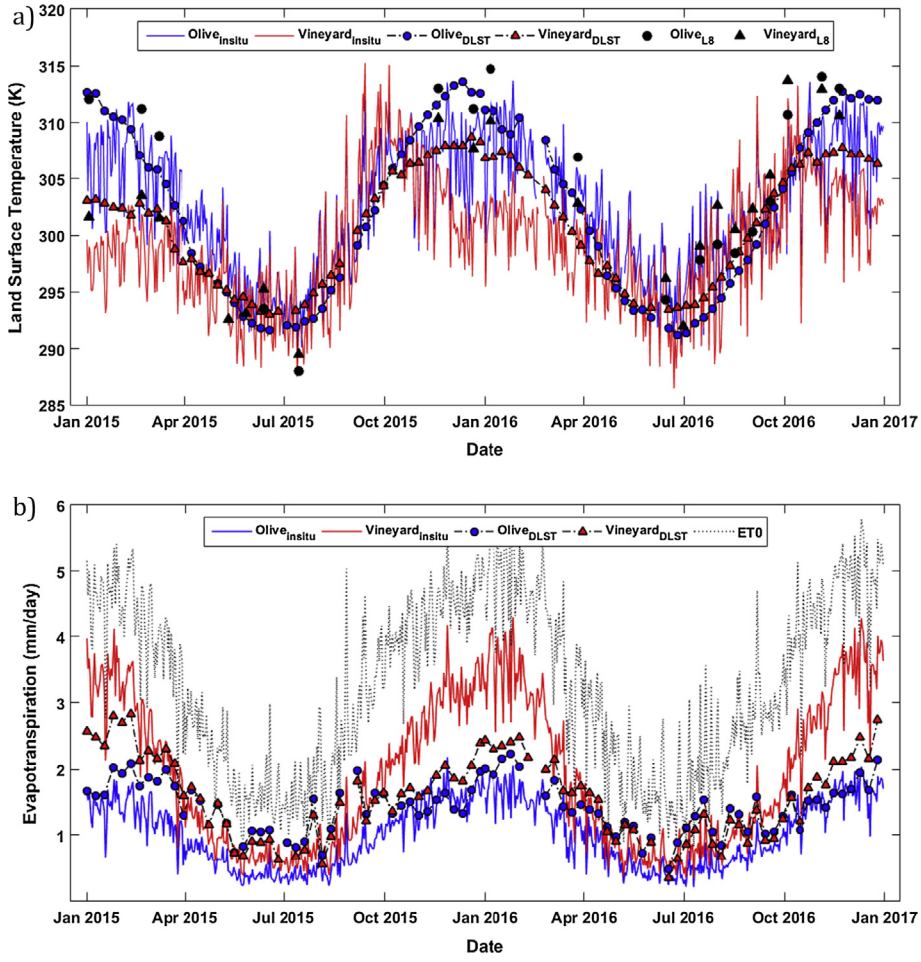

Fig. 8. Comparison between *DLST* and the in situ *LST* from LAB-net stations (top). LST from Landsat-8 overpass is shown for comparison for olives ($Olive_{L8}$) and vineyards ($Vineyard_{L8}$). Comparison between *ETa* from SSEBop and *DLST* and Kc-based ET (in situ) for olives orchards and vineyards (bottom).

Table 2
Coefficient of determination (r^2), mean bias error (Bias), standard deviation (Sigma) and root mean square error (RMSE) for *DLST* proposed and *ETa* from *DLST* and SSEBop method over olives orchards and vineyards. The values correspond to mean every 8 days at 100 m for the period 2015 to 2016. The same statistical parameters of LST and *ETa* from Landsat-8 are shown for comparison in the same period.

		Bias	Sigma	RMSE	r^2
DLST [K]	Olives	−0.30	3.56	3.57	0.87
	Vineyards	1.46	3.24	3.55	0.62
	Overall	0.59	3.50	3.55	0.72
LST Landsat-8 K	Olives	−0.37	3.29	3.31	0.95
	Vineyards	1.66	2.61	3.09	0.90
	Overall	0.72	3.08	3.16	0.87
ETa (DLST) [mm/day]	Olives	0.41	0.29	0.50	0.63
	Vineyards	−0.37	0.60	0.70	0.80
	Overall	0.02	0.61	0.61	0.67
ETa (Landsat-8) [mm/day]	Olives	0.27	0.41	0.49	0.44
	Vineyards	−0.52	0.77	0.93	0.63
	Overall	−0.15	0.74	0.75	0.49

to surface energy balance. These results are related to previous works which also demonstrate that the sinusoidal model can be used to obtain daily *LST* maps at medium spatial resolution (Weng et al., 2014). Moreover, based on the linear relationship derived from the interpolated sinusoidal regression coefficients, the *LST* can be obtained based on the *NDVI*, thus resulting in good seasonal performance over the arid area used here.

The *ETa* method for arid regions seems to be consistent with the results in terms of the operational algorithm and its retrievals. The *SSEBop* method is based on the differences between the dry and hot surface and air temperatures and in this context, the *DLST* method proposed here will be an excellent approach in terms of a good characterization of the *LST* over arid regions. This good characterization based on the combined ω fraction and *NDVI–LST* relationship represents the maximum and minimum of temperature used in the *dT* equation, a parameter which highly affects *ETa* retrievals during summer.

The *ETa* retrieved by the *DLST* obtained from the proposed method is consistent with the results when showing lower *ETa* than *ET0* values and is also influenced by the vegetation cover.

The phenology is a key parameter for a reliable *DLST* method and therefore the operation in terms of *ETa* maps. The validation was partially applied since the flooding that occurred in this area deserved more analysis to validate the *DLST* and *ETa* approach after September 2015, when the vineyards started the growing season. Nevertheless, the partial validation presented in this work demonstrates solid performance of the operational method in terms of *LST* and *ETa*.

Finally, several agricultural practices consider the *ET0* in this region in order to develop accurate water irrigation scheduling, which has overestimated the crop water requirements. Further efforts need to be applied to improve water use efficiency in the Copiapó Valley and should be accompanied by better knowledge of the crop spatial heterogeneity and a suitable strategy for an in situ monitoring network.

6. Conclusions

This work presents an operational method for disaggregating *LST* over an arid to semi-arid region that take into account (1) the spatial relationship between Landsat-8 and MODIS *LST*, (2) the spatial relationship between *LST* and the Normalized Difference Vegetation Index (*NDVI*) at high resolution (Landsat-8), and (3) the combination of both relationships. The disaggregated *LST* is integrated into an operational surface energy balance method (*SSEBop*) in order to estimate *ETa* at high temporal and spatial resolution. Results show that the developed approach gives an RMSE in *LST*, in average, lower than 3.6 K and an mean 8-day *ETa* lower than 0.7 mm/day. This approach is useful for generating better knowledge of water requirements in arid region which could be especially important in Chile where irrigation scheduling needs to be improved based on the current water usage and scarcity scenarios. Moreover, the proposed method modulates the contribution of vegetation by using two disaggregation methods based on temperature and *NDVI*. The simple use of *NDVI* and meteorologically-based equation could provide biased results since the values of *NDVI* need to be adapted to the high surface temperature derived from the soil/vegetation proportion. So, the use of integrated and operational method to extract surface information of surface and air temperature in addition to vegetation index could improve the surface energy balance in the arid region of Copiapó. Finally, this work contributes to determine and optimize the water demand in arid regions affected by the current drought in Chile, providing reliable *ETa* maps for irrigation scheduling and water use efficiency.

Acknowledgements

This work was partially funded by the projects Fondecyt-Initial (CONICYT/ref-11130359) and Fondef IDeA (CONICYT/ref-CA13I10102). The authors also wish to thank the NASA/MODIS and USGS/Landsat-8 teams for the data used in this work and also to Karina Palacios and Valentina Saavedra for their invaluable support in this work.

References

Agam, N., Kustas, W.P., Anderson, M.C., Li, F., Neale, C.M.U., 2007. A vegetation index based technique for spatial sharpening of thermal imagery. Remote Sens. Environ. 107, 545–558.

Allen, R.G., Pereira, L.S., Raes, D., Smith, M., 1998. Crop Evapotranspiration - Guidlines for Computing Crop Water Requirements. Irrig. Drainage. Pap. 56. Food Agriciculture. Organ., United Nations, Rome, Italy.

Allen, R.G., Pereira, L.S., Howell, T.a, Jensen, M.E., 2011. Evapotranspiration information reporting: I. Factors governing measurement accuracy. Agric. Water Manag. 98, 899–920. http://dx.doi.org/10.1016/j.agwat.2010.12.015.

Anderson, M.C., Norman, J.M., Mecikalski, J.R., Torn, R.D., Kustas, W.P., Basara, J.B., 2004. A multiscale remote sensing model for disaggregating regional fluxes to micrometeorological scales. J. Hydrometeorol. 5, 343–363. http://dx.doi.org/10.1175/1525-7541(2004)005<0343:AMRSMF>2.0.CO;2.

Anderson, M.C., Allen, R.G., Morse, A., Kustas, W.P., 2012. Use of Landsat thermal imagery in monitoring evapotranspiration and managing water resources. Remote Sens. Environ. 122, 50–65. http://dx.doi.org/10.1016/j.rse.2011.08.025.

Baldridge, A.M., Hook, S.J., Grove, C.I., Rivera, G., 2009. The ASTER spectral library version 2.0. Remote Sens. Environ 113, 711–715. http://dx.doi.org/10.1016/j.rse.2008.11.007.

Bastiaanssen, W.G.M., 1995. Regionalization of Surface Flux Densities and Moisture Indicators in Composite Terrain.

Bastiaanssen, W.G.M., Pelgrum, H., Wang, J., Ma, Y., Moreno, J.F., Roerink, G.J., van der Wal, T., 1998. A remote sensing surface energy balance algorithm for land (SEBAL). J. Hydrol. 212–213, 213–229. http://dx.doi.org/10.1016/S0022-1694(98)00254-6.

Bechtel, B., 2012. Robustness of annual cycle parameters to characterize the urban thermal landscapes. IEEE Geosci. Remote Sens. Lett. 9, 876–880. http://dx.doi.org/10.1109/LGRS.2012.2185034.

Bindhu, V.M., Narasimhan, B., Sudheer, K.P., 2013. Development and verification of a non-linear disaggregation method (NL-DisTrad) to downscale MODIS land surface temperature to the spatial scale of Landsat thermal data to estimate evapotranspiration. Remote Sens. Environ. 135, 118–129. http://dx.doi.org/10.1016/j.rse.2013.03.023.

Boisier, J.P., Rondanelli, R., Garreaud, R., Muñoz, F., 2016. Anthropogenic and natural contributions to the Southeast Pacific precipitation decline and recent megadrought in central Chile. Geophys. Res. Lett. http://dx.doi.org/10.1002/2015GL067265.

Bravo, D., 2013. Análisis de la incorporación de agua desalada al sistema hídrico en la cuenca del Río Copiapó. Memoria de Título. Universidad de Chile, Santiago, Chile, p. 60.

Cammalleri, C., Anderson, M.C., Gao, F., Hain, C.R., Kustas, W.P., 2014. Mapping daily evapotranspiration at field scales over rainfed and irrigated agricultural areas using remote sensing data fusion. Agric. For. Meteorol. 186, 1–11. http://dx.doi.org/10.1016/j.agrformet.2013.11.001.

Cheema, M.J.M., Bastiaanssen, W.G.M., 2010. Land use and land cover classification in the irrigated Indus Basin using growth phenology information from satellite data to support water management analysis. Agric. Water Manag. 97, 1541–1552. http://dx.doi.org/10.1016/j.agwat.2010.05.009.

Direccion General de Aguas, D., 2007. Estimaciones De Demanda De Agua Y Proyecciones Futuras. Zona II. Regiones V a XII y Región Metropolitana S.I.T. N° 122 571.

Duchemin, B., Goubier, J., Courrier, G., 1999. Monitoring phenological key stages and cycle duration of temperate deciduous forest ecosystems with NOAA/AVHRR data. Remote Sens. Environ. 67, 68–82. http://dx.doi.org/10.1016/S0034-4257(98)00067-4.

Durán-Alarcón, C., Santamaría-Artigas, A., Valenzuela, N., Mattar, C., 2014. RSR Calculator, una herramienta para el proceso de Calibración/Validación. Rev. Española Teledetec. 42, 111–117. http://dx.doi.org/10.4995/raet.2014.3230.

Findell, K.L., Gentine, P., Lintner, B.R., Kerr, C., 2011. Probability of afternoon precipitation in eastern United States and Mexico enhanced by high evaporation. Nat. Geosci. 4, 434–439. http://dx.doi.org/10.1038/ngeo1174.

Gao, Z., Gao, W., Chang, N.-B., 2011. Integrating temperature vegetation dryness index (TVDI) and regional water stress index (RWSI) for drought assessment with the aid of LANDSAT TM/ETM+ images. Int. J. Appl. Earth Obs. Geoinf. 13, 495–503. http://dx.doi.org/10.1016/j.jag.2010.10.005.

Guillevic, P.C., Biard, J.C., Hulley, G.C., Privette, J.L., Hook, S.J., Olioso, A., Göttsche, F. M., Radocinski, R., Román, M.O., Yu, Y., Csiszar, I., 2014. Validation of Land Surface Temperature products derived from the Visible Infrared Imaging Radiometer Suite (VIIRS) using ground-based and heritage satellite measurements. Remote Sens. Environ. 154, 19–37. http://dx.doi.org/10.1016/j.rse.2014.08.013.

Hong, S., Hendrickx, J.M.H., Borchers, B., Science, E., 2011. Down-scaling of SEBAL derived evapotranspiration maps from MODIS (250 m) to Landsat (30 m) scales. Earth 32, 1–37. http://dx.doi.org/10.1080/01431161.2010.512929.

Hulley, G., Hook, S., 2013. The ASTER Global Emissivity Database (ASTER GED) Collection.

Jiménez-Muñoz, J.C., Sobrino, J.A., Mattar, C., Franch, B., 2010. Atmospheric correction of optical imagery from MODIS and Reanalysis atmospheric products. Remote Sens. Environ. 114, 2195–2210. http://dx.doi.org/10.1016/j.rse.2010.04.022.

Jiménez-Muñoz, J.C., Sobrino, J.A., Skokovi, D., Mattar, C., Cristóbal, J., 2014. Land surface temperature retrieval methods from Landsat-8 thermal infrared sensor data. Geosci. Remote Sens. Lett. IEEE 11, 1840–1843. http://dx.doi.org/10.1109/LGRS.2014.2312032.

Kalma, J.D., McVicar, T.R., McCabe, M.F., 2008. Estimating land surface evaporation: a review of methods using remotely sensed surface temperature data. Surv. Geophys. 29, 421–469. http://dx.doi.org/10.1007/s10712-008-9037-z.

Kim, J., Hogue, T.S., 2012. Evaluation and sensitivity testing of a coupled Landsat-MODIS downscaling method for land surface temperature and vegetation indices in semi-arid regions. J. Appl. Remote Sens. 6, 63517–63569. http://dx.doi.org/10.1117/1.JRS.6.063569.

Kustas, W.P., Norman, J.M., Anderson, M.C., French, A.N., 2003. Estimating subpixel surface temperatures and energy fluxes from the vegetation index–radiometric temperature relationship. Remote Sens. Environ. 85, 429–440. http://dx.doi.org/10.1016/S0034-4257(03)00036-1.

Li, Z.-L., Tang, R., Wan, Z., Bi, Y., Zhou, C., Tang, B., Yan, G., Zhang, X., 2009. A review of current methodologies for regional evapotranspiration estimation from

remotely sensed data. Sensors (Basel) 9, 3801–3853. http://dx.doi.org/10.3390/s90503801.

Li, M., Qu, J.J., Hao, X., 2010. Investigating phenological changes using MODIS vegetation indices in deciduous broadleaf forest over continental U.S. during 2000–2008. Ecol. Inform. 5, 410–417. http://dx.doi.org/10.1016/j.ecoinf.2010.04.002.

Li, Z.-L., Tang, B.-H., Wu, H., Ren, H., Yan, G., Wan, Z., Trigo, I.F., Sobrino, J.A., 2013. Satellite-derived land surface temperature: current status and perspectives. Remote Sens. Environ. 131, 14–37. http://dx.doi.org/10.1016/j.rse.2012.12.008.

Liu, Y., Hill, M.J., Zhang, X., Wang, Z., Richardson, A.D., Hufkens, K., Filippa, G., Baldocchi, D.D., Ma, S., Verfaillie, J., Schaaf, C.B., 2017. Using data from Landsat, MODIS, VIIRS and PhenoCams to monitor the phenology of California oak/grass savanna and open grassland across spatial scales. Agric. For. Meteorol. 237–238, 311–325. http://dx.doi.org/10.1016/j.agrformet.2017.02.026.

Martínez, L., Tapia, F., 2002. Riego del Olivar Proyecto: Manejo Moderno de Huertos de Olivos en el Valle de Huasco Bol. INIA N°72 34.

Mattar, C., Franch, B., Sobrino, J.A., Corbari, C., Jiménez-Muñoz, J.C., Olivera-Guerra, L., Skokovic, D., Sória, G., Oltra-Carriò, R., Julien, Y., Mancini, M., 2014. Impacts of the broadband albedo on actual evapotranspiration estimated by S-SEBI model over an agricultural area. Remote Sens. Environ. 147, 23–42. http://dx.doi.org/10.1016/j.rse.2014.02.011.

Mattar, C., Durán-Alarcón, C., Jimenez-Munoz, J.C., Santamaría-Artigas, A., Olivera-Guerra, L., Sobrino, J.A., 2015. Global Atmospheric Profiles from Reanalysis Information (GAPRI): a new database for earth surface temperature retrieval. Int. J. Remote Sens. 37–41. http://dx.doi.org/10.1080/01431161.2015.1054965.

Mattar, C., Santamaría-artigas, A., Durán-alarcón, C., Olivera-guerra, L., Fuster, R., Borvarán, D., 2016. The LAB-net soil moisture network : application to thermal remote sensing and surface energy balance. Data 1, 1–14. http://dx.doi.org/10.3390/data1010006.

Merlin, O., Duchemin, B., Hagolle, O., Jacob, F., Coudert, B., Chehbouni, G., Dedieu, G., Garatuza, J., Kerr, Y., 2010. Disaggregation of MODIS surface temperature over an agricultural area using a time series of Formosat-2 images. Remote Sens. Environ. 114, 2500–2512. http://dx.doi.org/10.1016/j.rse.2010.05.025.

Merlin, O., Jacob, F., Wigneron, J.P., Walker, J., Chehbouni, G., 2012. Multidimensional disaggregation of land surface temperature using high-resolution red, near-infrared, shortwave-infrared, and microwave-L bands. IEEE Trans. Geosci. Remote Sens. 50, 1864–1880. http://dx.doi.org/10.1109/TGRS.2011.2169802.

Mukherjee, S., Joshi, P.K., Garg, R.D., 2014. A comparison of different regression models for downscaling Landsat and MODIS land surface temperature images over heterogeneous landscape. Adv. Sp. Res. 54, 655–669. http://dx.doi.org/10.1016/j.asr.2014.04.013.

Nemani, R.R., Pierce, L., Running, S.W., Goward, S., 1993. Developing satellite-derived estimates of surface moisture stress. J. Applied Met. 32, 548–557. http://dx.doi.org/10.1175/1520-0450.

Ogawa, K., Schmugge, T., Jacob, F., 2003. Estimation of land surface window (8–12 μm) emissivity from multi-spectral thermal infrared remote sensing — a case study in a part of Sahara Desert. Geophys. Res. Lett. 30 (2), 12–15. http://dx.doi.org/10.1029/2002GL016354.

Oki, T., Kanae, S., 2006. Global hydrological cycles and world water resources. Science 313, 1068–1072. http://dx.doi.org/10.1126/science.1128845 (80-.).

Olivera-Guerra, L., Mattar, C., Durán-Alarcón, C., Santamaría-Artigas, A., Fuster, R., 2014. A first evaluation of an operational method to estimate actual evapotranspiration by using MODIS data over the semi-arid region of Chile. In: Procd. IV Recent Advances in Quantitative Remote Sensing Symposium (RAQRS). 22–25 September, Valencia, Spain.

Oyarzún, J., Oyarzún, R., 2011. Sustainable development threats, inter-sector conflicts and environmental policy requirements in the arid, mining rich, Northern Chile territory. Sustain. Dev. 19, 263–274. http://dx.doi.org/10.1002/sd.441.

Porter, D.O., Gowda, P.H., Marek, T.H., Howell, T.A., Irmak, S., Moorhead, J., 2012. Sensitivity of grass and alfalfa reference evapotranspiration to sensor accuracy. Appl. Eng. Agric. 28, 543–549. http://dx.doi.org/10.1007/s00382-007-0340-z.

Prata, A.J., Caselles, V., Coll, C., Sobrino, J.A., Ottle, C., 1995. Thermal remote sensing of land surface temperature from satellites: current status and future prospects. Remote Sens. Rev. 12 (3–4), 175–224. http://dx.doi.org/10.1080/02757259509532285.

Rousseeuw, P.J., 1984. Least median of squares regression. J. Am. Stat. Assoc. 79, 871–880.

Senay, G.B., Bohms, S., Singh, R.K., Gowda, P.H., Velpuri, N.M., Alemu, H., Verdin, J.P., 2013. Operational evapotranspiration mapping using remote sensing and weather datasets: a new parameterization for the SSEB approach. JAWRA J. Am. Water Resour. Assoc. 49, 577–591. http://dx.doi.org/10.1111/jawr.12057.

Senay, G.B., Friedrichs, M., Singh, R.K., Velpuri, N.M., 2016. Evaluating Landsat 8 evapotranspiration for water use mapping in the Colorado River Basin. Remote Sens. Environ. 185, 171–185. http://dx.doi.org/10.1016/j.rse.2015.12.043.

Sobrino, J.A., Li, Z.L., Stoll, M.P., Becker, F., 1996. Multi-channel and multi-angle algorithms for estimating sea and land surface temper- ature with ATSR data. Int. J. Remote Sens. 17 (11), 2089–2114.

Sobrino, J.A., Jiménez-muñoz, J.C., Sòria, G., Romaguera, M., Guanter, L., Moreno, J., Member, A., Plaza, A., Member, S., Martínez, P., 2008. Land surface emissivity retrieval from different VNIR and TIR sensors. IEEE Trans. Geosci. Remote Sens. 46, 316–327.

Sobrino, J.A., Franch, B., Mattar, C., Jiménez-Muñoz, J.C., Corbari, C., 2012. A method to estimate soil moisture from Airborne Hyperspectral Scanner (AHS) and ASTER data: application to SEN2FLEX and SEN3EXP campaigns. Remote Sens. Environ. 117, 415–428. http://dx.doi.org/10.1016/j.rse.2011.10.018.

Suarez, F., Muñoz, J.F., Fernández, B., Dorsaz, J.-M., Hunter, Ch., Karavitis, C.A., Gironás, J., 2014. Integrated water resource management and energy requirements for water supply in the Copiapó River Basin, Chile. Water 6, 2590–2613.

Valdés-Pineda, R., Pizarro, R., García-Chevesich, P., Valdés, J., Olivares, C., Vera, M., Balocchi, F., Pérez, F., Vallejos, C., Fuentes, R., Abarza, A., Helwig, B., 2014. Water governance in Chile: availability, management and climate change. J. Hydrol. 519 (Part C), 2538–2567.

Vauclin, M., Vieira, R., Bernard, R., Hatfield, J.L., 1982. Spatial variability of surface tem- perature along two transects of a bare. Water Resour. Res. 18, 1677–1686.

Weng, Q., Fu, P., Gao, F., 2014. Generating daily land surface temperature at Landsat resolution by fusing Landsat and MODIS data. Remote Sens. Environ. 145, 55–67. http://dx.doi.org/10.1016/j.rse.2014.02.003.

Weng, Q., Liu, H., Liang, B., Lu, D., 2008. The spatial variations of urban land surface temperatures: pertinent factors, zoning effect, and seasonal variability. IEEE J. Sel. Top. Appl. Earth Obs. Remote Sens. 1, 154–166. http://dx.doi.org/10.1109/JSTARS.2008.917869.

Zhan, W., Chen, Y., Zhou, J., Wang, J., Liu, W., Voogt, J., Zhu, X., Quan, J., Li, J., 2013. Disaggregation of remotely sensed land surface temperature: literature survey, taxonomy, issues, and caveats. Remote Sens. Environ. 131, 119–139. http://dx.doi.org/10.1016/j.rse.2012.12.014.

Zhu, X., Chen, J., Gao, F., Chen, X., Masek, J.G., 2010. An enhanced spatial and temporal adaptive reflectance fusion model for complex heterogeneous regions. Remote Sens. Environ. 114, 2610–2623. http://dx.doi.org/10.1016/j.rse.2010.05.032.